



HAL
open science

Analysis of the long term interaction between molten core and dry concrete at Fukushima Daiichi Unit 1

Marco Pellegrini, Christophe Journeau, Nathalie Seiler, Luis Enrique Herranz, Claus Spengler, Charline Bouillet, Marc Barrachin, David Luxat, Lucas Allbright

► To cite this version:

Marco Pellegrini, Christophe Journeau, Nathalie Seiler, Luis Enrique Herranz, Claus Spengler, et al.. Analysis of the long term interaction between molten core and dry concrete at Fukushima Daiichi Unit 1. NURETH 20 - 20th International Topical Meeting on Nuclear Reactor Thermal Hydraulics, ANS - American Nuclear Society, Aug 2023, Washington DC, United States. pp.Special Session: OECD/NEA ARC-F and PreADES Projects: I. cea-04237542

HAL Id: cea-04237542

<https://cea.hal.science/cea-04237542>

Submitted on 11 Oct 2023

HAL is a multi-disciplinary open access archive for the deposit and dissemination of scientific research documents, whether they are published or not. The documents may come from teaching and research institutions in France or abroad, or from public or private research centers.

L'archive ouverte pluridisciplinaire **HAL**, est destinée au dépôt et à la diffusion de documents scientifiques de niveau recherche, publiés ou non, émanant des établissements d'enseignement et de recherche français ou étrangers, des laboratoires publics ou privés.

Copyright

Analysis of the Long Term Interaction Between Molten Core And Dry Concrete At Fukushima Daiichi Unit 1

M. Pellegrini

The University of Tokyo
Corresponding Address
marco@n.t.u-tokyo.ac.jp

C. Journeau, N. Seiler

CEA, IRESNE, DTN, SMTA, Cadarache, F-13108 Saint-Paul-lez-Durance
Christophe.journeau@cea.fr; Nathalie.SEILER@cea.fr

L.E. Herranz

CIEMAT
Address Avda. Complutense, 40 28040 Madrid, SPAIN
luisen.herranz@ciemat.es

C. Spengler

Gesellschaft für Anlagen- und Reaktorsicherheit (GRS) gGmbH
claus.spengler@grs.de

C. Bouillet, M. Barrachin

Institut de Radioprotection et de sûreté Nucléaire (IRSN)
31, avenue de la division Leclerc, Fontenay-aux-Roses, 92260, France
charlaine.bouillet@irsn.fr; marc.barrachin@irsn.fr

D. Luxat, L. Albright

Sandia National Lab
dlluxat@sandia.gov

ABSTRACT

The latest investigations of Fukushima Daiichi Unit 1 have demonstrated that corium attack to the pedestal walls and pedestal floor has occurred in Fukushima Daiichi Unit 1 to a certain extent. The results of past analytical benchmarks such as the OECD/NEA BSAF project were in agreement with this finding. However, the latest investigation do not show evidence of unlimited MCCI which is one of the main discrepancies from the BSAF project. More recently a MCCI benchmark has been launched in the context of the OECD/NEA ARC-F project. In the benchmark, common geometry, boundary and initial conditions have been selected among all the participants. The results show an improved agreement among different codes for what concerns overall erosion, corium temperature and hydrogen generation, however the unlimited erosion is still predicted by all codes. It is considered that this behavior might be the result of improper boundary conditions or modeling (e.g. interfacial temperature and effective heat transfer coefficients) In this paper, a summary of the overall results and a discussion of modeling and boundary conditions is done to disclose the results of the activity and the future steps to be taken in the OECD/NEA FACE project.

KEYWORDS

Fukushima Daiichi, MCCI, corium, concrete, benchmark, OECD/NEA ARC-F

1. INTRODUCTION

As of today, it has been over ten years since the accident occurred at Fukushima Daiichi Nuclear Power Station (NPS). Since then, the analyses of the accident have multiplied and it has been performed in a variety of ways from analytical, experimental, and computational. The legacy work of computational analysis of the accident by mean of Severe Accident (SA) codes is represented by the OECD/NEA Benchmark Study of the Accident at Fukushima Daiichi NPS (BSAF) Phase 1 and Phase 2 [1][2][3][4]. The project highlighted uncertainties to what concerns in-vessel core degradation, such as accumulation of debris on core plate, melt of BWRs internal structures (e.g. separators and dryers) and the possibility of the generation of volatile boric acid. In addition, one striking result of the BSAF activity was the extensive progression of MCCI for all codes with continuous erosion until 500 h, which is not confirmed by any indirect evidence at the plant. In Phase 2 a number of uncertainties still existing to what concerns Fission Products (FP) behavior is also extensively covered in the activity.

Recent inspections (in May 2022) of Fukushima Daiichi Unit Primary Containment Vessel (PCV) in Unit 1 has provided the final direct evidence that the overall MCCI progression represents a misprediction, hence the final shape of the eroded cavity might appear different from what estimated by SA codes. The inspection has also introduced additional points of reflection not considered in the past, for example the creation of layers of debris outside the pedestal and the creation of certain concrete areas where the cement paste disintegrates while the rebars are relatively intact.

In a subsequent project of the OECD/NEA named Analysis of Information from Reactor Buildings and Containment Vessels of Fukushima Daiichi Nuclear Power Station (ARC-F) some of the issues identified in the BSAF project were further investigated by sub-groups who are given the freedom to organize activities to clarify the remaining issues. In particular, Group 3 was dedicated to the MCCI analysis targeting the issue of unlimited concrete erosion. The Group 3 saw the participation of 7 organizations, namely CEA, CIEMAT, GRS, IAE, IBRAE, IRSN and NRA, all of them were previously participating in the BSAF project. The group is organized by the University of Tokyo.

The activity was organized similarly to what done for in-vessel degradation between the MAAP and MELCOR code and named Crosswalk [5]. Namely, geometry, boundary and initial conditions were agreed by all the participants and evaluated based on existing data or previous analysis of the BSAF project. In this particular exercise the power removed at the top boundary, which represents the only energy loss has been fixed with a realistic shape for all the computations. Primary data of concrete erosion vertically and radially and debris temperature are requested, as well as secondary data represented by heat fluxes from the debris (e.g. radiation, convection) which are considered necessary for a thorough evaluation of the computation. The modeling of the heat transfer network has been investigated between different codes in order to highlight differences in the erosion pattern.

2. SUMMARY OF THE BSAF PHASE 2 MCCI PROGRESSION (UNIT 1)

Results of the vertical erosion for the BSAF phase 2 are reported in Figure 1 and discussed in detail in [2]. Except few outliers the similarities reported in Table I regarding the initial discharge of corium debris and the initial corium mass are reflected in a relatively similar trend of the concrete erosion in the vertical direction (Figure 1 a), while larger discrepancies exist in the lateral erosion (Figure 1 b). Calculations like IRSN show a larger mass because they include also a considerable mass of structures belonging to the lower plenum.

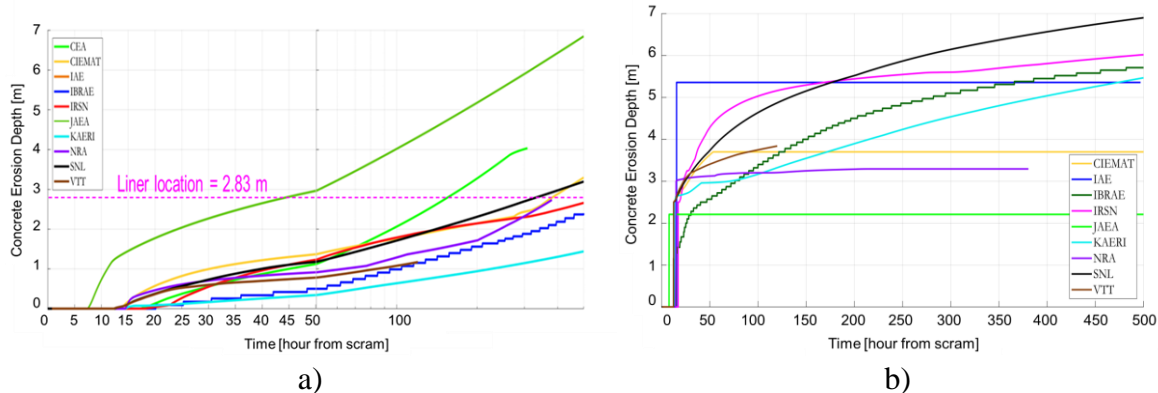


Figure 1 BSAF phase 2 results of the MCCI vertical erosion for Unit 1 [[2]]

As presented in the vertical erosion all calculations show a continuous concrete erosion up to 270 h, time when the MCCI progression is considered dry, i.e. no water injection. In addition all codes, except CEA, show a negligible effect of the water injection as the erosion continues beyond 270 h, until 500 h, when alternative water injection becomes effective.

Table I RPV failure time and total initial debris mass in pedestal (Unit 1) [[2]]

	CEA	CIEMAT	IAE	IBRAE	IRSN	JAEA	KAERI	NRA ¹	SNL	VTT
RPV failure [h]	N/A	11.58	14.97	15.10	17.16	7.45	13.50	13.6	12.5	11.42
Total masses in pedestal [ton]	39 ²	129	148	196	282	130	136	115	154	111

In the activity proposed in Group 3 of the ARC-F it was decided to evaluate the codes' response to a simplified geometry (i.e. one single sump) with controlled initial and boundary conditions in a dry MCCI progression (i.e. no water injection). The objective of the activity is to confirm the general tendency of the codes to compute an unlimited concrete erosion and individuate the main responsible models and parameters.

3. ARC-F GROUP 3 SPECIFICATIONS

3.1. Geometry

The geometry decided for the benchmark is one of the two sumps existing in the pedestal. Sumps are used to accumulate water dripping from the lower head during normal operation. Heat exchangers exist in the sump to cool down the accumulated water. Sumps are considered as the main source of MCCI since the large volume to surface ratio generates an almost uncoolable geometry. The dimensions of the sump are reported in Figure 2. The debris is injected in the middle of the sump. In case any of the codes accounted for debris swelling due to gas generation it was allowed to increase the height of the sump enough to avoid overflowing of the debris.

¹ NRA total masses do not include SS and SSOx

² This value includes only the debris mass in two sumps since CEA calculation with TOLBIAC considers only the sumps. It does not consider the mass above the pedestal and D/W floor.

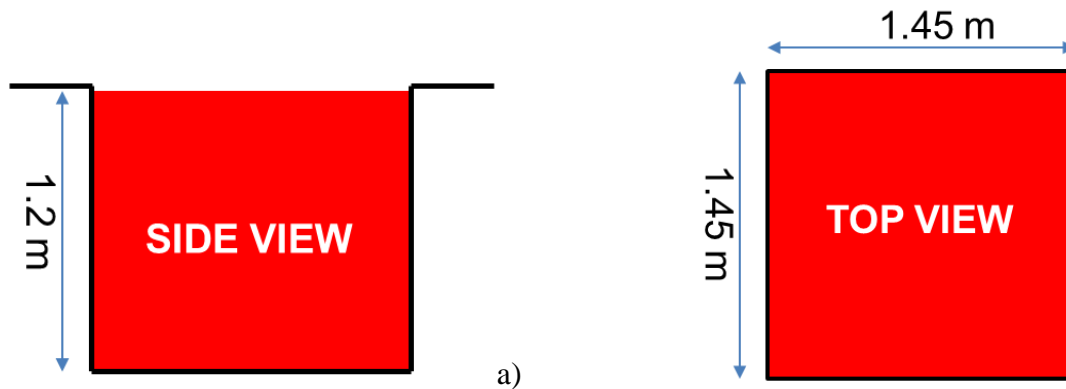


Figure 2 Geometry to be studied in the ARG-F benchmark of Group 3. a) shows the side view and b) shows the top view.

3.2. Boundary and Initial Conditions

The calculation is assumed to start at time 12.5 h with the debris injection instantaneous at this time. The problem is simulated until 270 h without any water injection. No stratification is assumed in the debris. The cavity pressure is assumed equal to 0.7 MPa and the gas temperature equal to 438.0 K.

3.2.1. Initial debris composition

The initial mass and composition of the debris is fundamental to define the amount of oxidation that takes place in the calculation and the overall properties of the corium. The initial composition depends on the history of the core degradation computed by each code, hence it is not a known value. In addition the composition of the stainless steel and its oxide form is fundamental to control the oxidation processes and not known a priori. In benchmark it was agreed to employ the values of SNL MELCOR code provided in the analysis of Unit 1 during the BSAF as representative of the plausible accident scenario. The values are presented in Table II and Table III.

Table II Debris mass composition employed in the ARC-F Group 3 benchmark

Component	Mass [kg]
SS	5380.60
SSO_x	458.63
Zr	2106.67
ZrO₂	2356.24
UO₂	9222.18
Tot	19524.32

Table III Stainless steel and stainless steel oxide composition employed in the ARC-F Group 3 benchmark

	Element	Mass [kg]	Percent
SS	Cr	1100.00	20.4%
	Ni	471.70	8.8%
	Fe	3808.90	70.8%
SSO_x	FeO	363.60	79.3%
	Cr ₂ O ₃	47.52	10.4%
	NiO	47.52	10.4%

The initial temperature of the debris is assumed following the data of SNL as 1481.346 K. The density is evaluated, based on the overall composition equal to 7647.306 kg/m³.

3.2.2. Initial concrete composition and properties

The initial composition of the concrete of Fukushima Daiichi was investigated by local inspection after the accident and reported by JAEA and CEA as the one in Table IV. As reported the concrete in Fukushima Daiichi is a basaltic composition. Basaltic concrete, as well as silicious one, does not contain CO₂ hence during the degradation and decomposition only steam is released in a minor quantity. Even though still uncertainties still remain, this characteristics of basaltic concrete (and silicious) create a preferential erosion laterally rather than vertically which could harm the structures in containment such as the one of Mark I with a narrow pedestal holding the pressure vessel [6].

Table IV Fukushima Daiichi Unit 1 concrete composition

Compounds	Al₂O₃	CaO	SiO₂	H₂O	Fe₂O₃
Weight (%)	15.4%	12.8%	62.5%	3.3%	6.0%

The rebar content is more complicated to be evaluated as this value changes depending on the location in the pedestal as some structures are more reinforced than others. The evaluation has been done by NRA and a value of 3.8% based on weight has been selected an average value, while the range of reinforcement is estimated to be between 1.0% to 12.0%. The concrete ablation temperature and energy have been evaluated by IRSN based on the concrete composition reported above. The ablation temperature was evaluated as 1541.0 K and the ablation energy as 1,778.539 J/kg. It should be noticed that the ablation energy includes also the sensible heat to increase the temperature of the concrete from the temperature of 300K to the ablation temperature. The initial concrete temperature is assumed as 300 K. Density is assumed in all calculations equal to 2400 kg/m³.

3.2.3. Decay heat

The decay heat has to account for the mass of volatile FPs which are released from the fuel during heat up, mostly noble gases, cesium and iodine. As presented in the BSAF project this amount is lower than 100% hence it cannot be evaluated analytically. For simplification also for this value the data computed during the BSAF phase 2 project by SNL are taken as reference. SNL provided the total decay heat in the pedestal, which has been normalized depending on the mass of debris contained in a single sump. The values are reported in Figure 3.

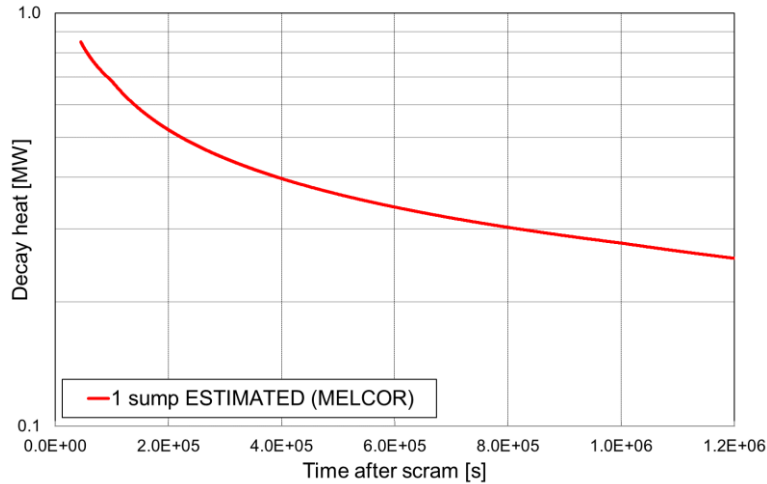


Figure 3 Decay heat of debris in a single sump based on SNL calculations

3.2.4. Power loss at the top surface

In order to make sure that boundary conditions are exactly the same for all the codes, it was decided to impose also the top boundary heat loss. As every code considers the contribution for the top heat loss differently (a combination of radiation and convection) it was not possible to fix the physical parameters, such as the surrounding temperature and emissivities. This curve was estimated by SNL based on their previous BSAF analyses.

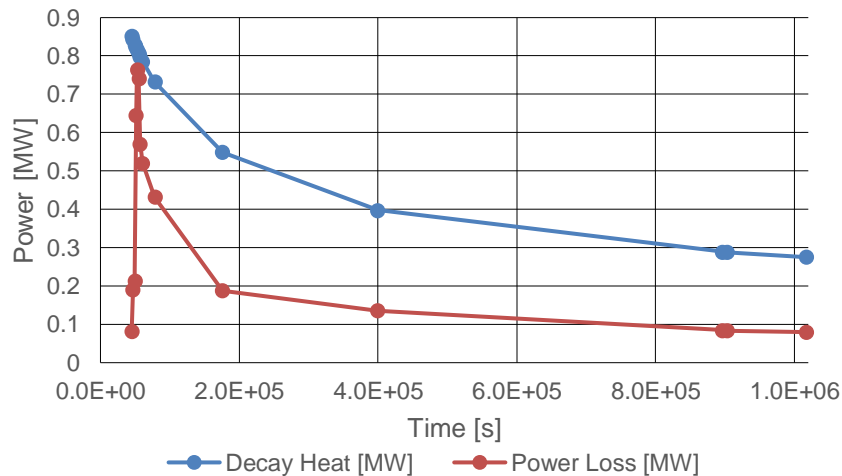


Figure 4 Decay heat and top boundary power loss imposed in the simulation

The heat loss curve is presented in Figure 4 in comparison with the decay heat and it shows that the imposed heat loss is always smaller than the decay heat.

4. DETAILS OF THE CODES MODELING

4.1. Heat Transfer Network

The codes employed by the participants in the exercise are presented in the table below:

Table V Summary of codes and institutes participating in the OECD/NEA ARC-F project

CODE NAME	INSTITUTE
ASTEC/MEDICIS	IRSN (France)
TOLBIAC-ICB	CEA (France)
AC ² /COCOSYS	GRS (Germany)
MELCOR/CORQUENCH	SNL (US), CIEMAT (Spain), NRA (Japan)

In the calculations, the temperature evolutions and ablation rate depend among other things on the definition of the boundary conditions which are quite different from each code.

The ASTEC/MEDICIS code models a slag layer, which is assumed in the lateral and bottom direction, in contact with the concrete (Figure 5 a). The temperature between the slag layer and the concrete is fixed to the ablation temperature ($T_{ablation}$) which is set as input and provided in the benchmark (3.2.2).

The overall heat balance is controlled by the heat transfer network assuming two different Heat Transfer Coefficients (HTC) for the slag (h_{slag}) and the convective pool (h_{conv}). Hence, an effective HTC is defined as:

$$h_{eff} = \frac{1}{\frac{1}{h_{conv}} + \frac{1}{h_{slag}}} \quad (1)$$

The MCCI model in AC²/COCOSYS is similar but uses an even more simplified approach, according to which the effective HTC is not provided by Eq. (1) but provided as constant input parameter. The latter approach assumes that $h_{slag} \ll h_{conv}$, so that the impact of h_{conv} may be neglected in Eq (1). In the benchmark calculations performed in Group 3 of the ARC-F consortium, the slag HTC in MEDICIS is assumed at a constant value of 300 W/m²K while the convective HTC is based on the BALI experiments [8][9] and in AC² h_{eff} was assumed 100 W/m²K.

For the heat balance on the top surface the computation is slightly more complicated, and it involves two cases presented in Figure 5 b and c. Initially, the crust is not existing in the codes ASTEC/MEDICIS and AC²/COCOSYS and the heat flux is dependent on the convective HTC to the top surface and the temperature difference between the convective pool and the top surface (T_{top}). However, in case the T_{top} falls below the solidification temperature, a crust is formed; the interface temperature, T_{int} (between the pool and the crust) is assumed to be equal to this solidification temperature. The conduction through the crust is then considered.

In AC² the solidification temperature is assumed to be equal to the solidus temperature, whereas in MEDICIS the solidification temperature is evaluated according to the value of the threshold liquid volume fraction equal to 50%.

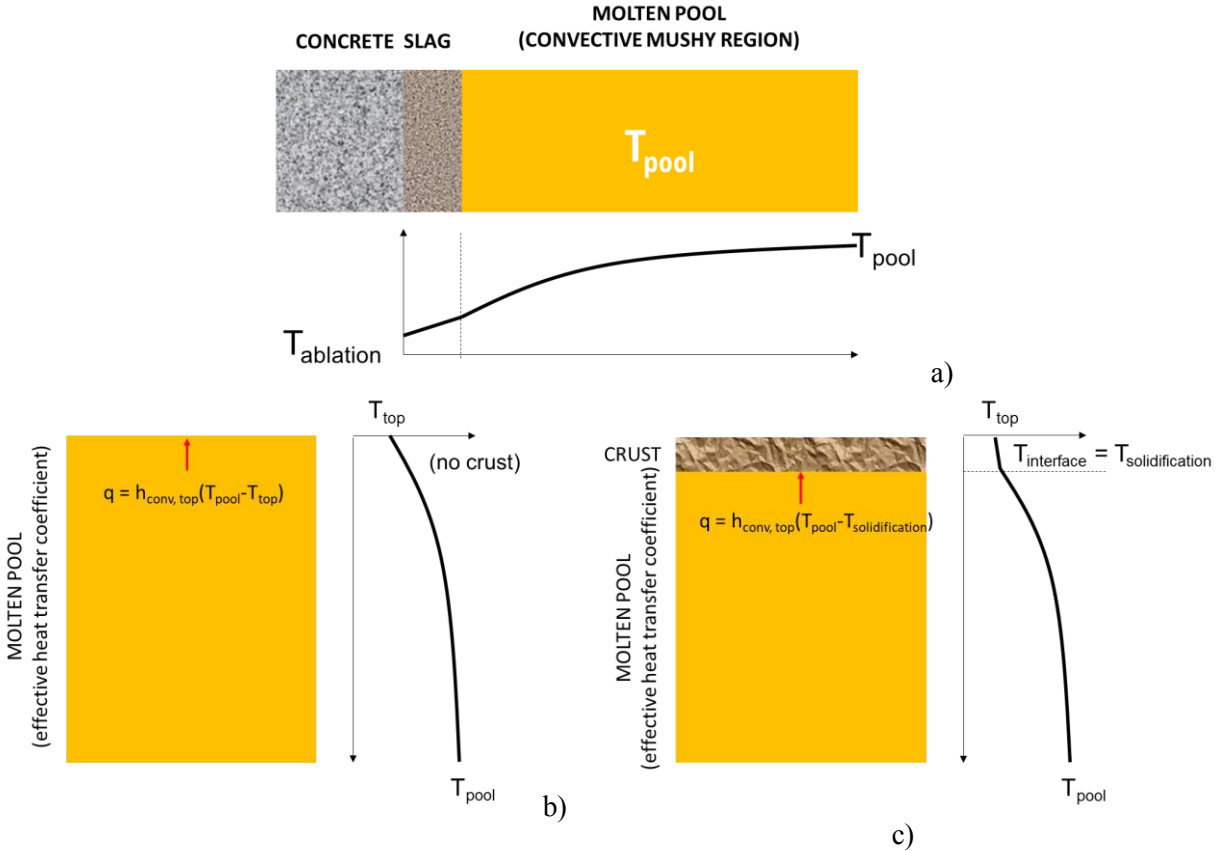


Figure 5 Schematic view of the heat transfer network employed in the ASTEC/MEDICIS code and the COCOSYS/AC² code. a) heat balance on the concrete side, b) and c) the two different states on the top surface

In the TOLBIAC-ICB code, the crust model assumes the thermodynamic equilibrium between the crusts and the molten pool. The main hypotheses of the model are that due to the high liquidus temperature of oxide melts and, despite the melting of concrete and the presence of gas issued from concrete decomposition, a solid crust is assumed to deposit at the concrete wall. The pool/crust interface temperature is equal to the liquidus temperature at the pool composition and the composition of the crust increment is that of the solid in equilibrium with the liquid pool composition (Figure 6). It must be noted that the decay power in that crust is taken into account. For a transient lasting several days, the crust thickness becomes large and this phenomenon is not negligible [6].

In TOLBIAC-ICB, the heat transfer at the pool/concrete interface is hence computed considering the convective heat flux from the pool at T_{pool} to the interface at $T_{liquidus}$ (whose convective heat transfer is given by BALI correlations [8][9]) and the released decay power inside the formed crust. Indeed, the convective heat coefficient in the pool is balanced by a reduced temperature difference between the pool and the liquidus temperature, compared to other codes for which this temperature difference is much larger. In a sense, this approach is similar to MEDICIS and the AC², when only looking at the molten pool side (the convective heat coefficients are derived from BALI experiments). However, the interface temperature between the pool and the crust is fixed to $T_{liquidus}$ in TOLBIAC-ICB, while it is an intermediate temperature between $T_{solidus}$ and $T_{liquidus}$ in the case of MEDICIS and AC² between the pool and the concrete which is computed by the code depending on the pool composition.

The heat transfer at the pool/top interface also involves a crust model on the top surface as in the MEDICIS and the AC² code, but in TOLBIAC-ICB this crust already exists from the beginning of the transient. Moreover, another difference is that the interface temperature between pool and the upper crust is not $T_{solidification}$ as MEDICIS and the AC² codes but once again $T_{liquidus}$. Slag layer is not considered because the temperature on the concrete boundary is assumed to be the liquidus temperature as presented in Figure 6.

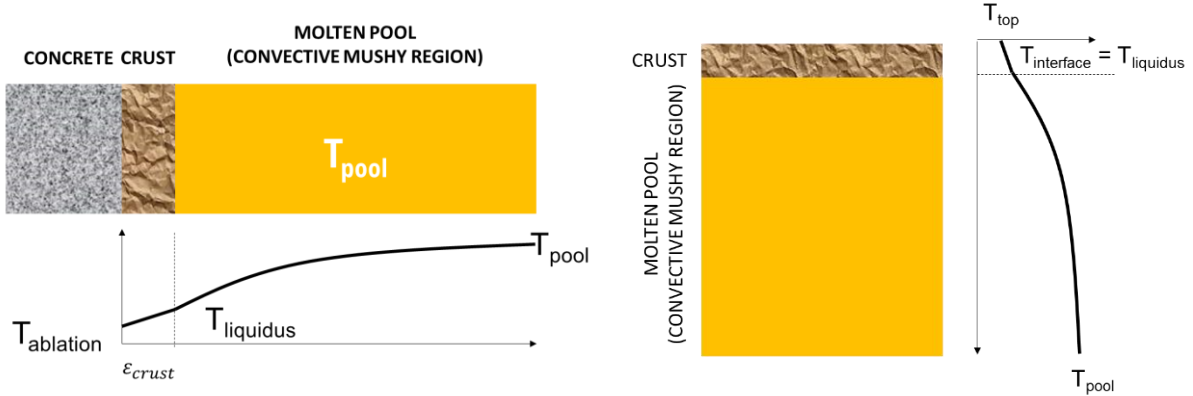


Figure 6 Schematic view of the heat transfer network employed in the TOLBIAC-ICB code

4.2. Ablation Velocity

The main result of the MCCI is represented by the ablation velocity, which is also the main variable to investigate the reason of endless erosion in the BSAF-2 results and the motivation for this exercise. In the same way as for the heat transfer network, the ablation velocity models of MEDICIS and AC² are consistent together, while TOLBIAC-ICB employs a slightly different definition. The ablation velocity for the first two codes is presented in equation (2)

$$v_{ablation} = \frac{dx_{ablation}}{dt} = \frac{h_{eff}(T_{pool} - T_{ablation})}{\Delta H_{abl} \rho_{s,conc}} \quad (2)$$

where h_{eff} is the effective HTC, ΔH_{abl} is the ablation concrete energy defined as:

$$\Delta H_{abl} = h_{conc}(T_{ablation}) - h_{conc}(T_0) \text{ with } T_0 = 300 \text{ K}$$

$h_{conc}(T_{ablation})$ is the specific enthalpy of the concrete at $T_{ablation}$ and $h_{conc}(T_0)$ the specific enthalpy of the concrete at T_0 . The $\rho_{s,conc}$ is the density of the solid concrete. The ablation energy provided in the exercise is effectively defined as above, hence including the sensible heat and the phase change.

On the other hand, the definition in TOLBIAC-ICB is relatively different and is expressed in equation (3) :

$$v_{ablation} = \frac{dx_{ablation}}{dt} = \frac{\varphi_{towards\ concrete}}{\Delta H_{abl} \rho_{s,conc} + \rho_{l,conc} c_{pl,conc} (T_{pool} - T_{abl})} \quad (3)$$

This expression comes from an energy balance on the concrete whose enthalpy, receiving the heat flux $\varphi_{towards\ concrete}$ (W/m²), evolves from $h_{conc}(T_0)$ at solid state to $h_{conc}(T_{pool})$ at liquid state.

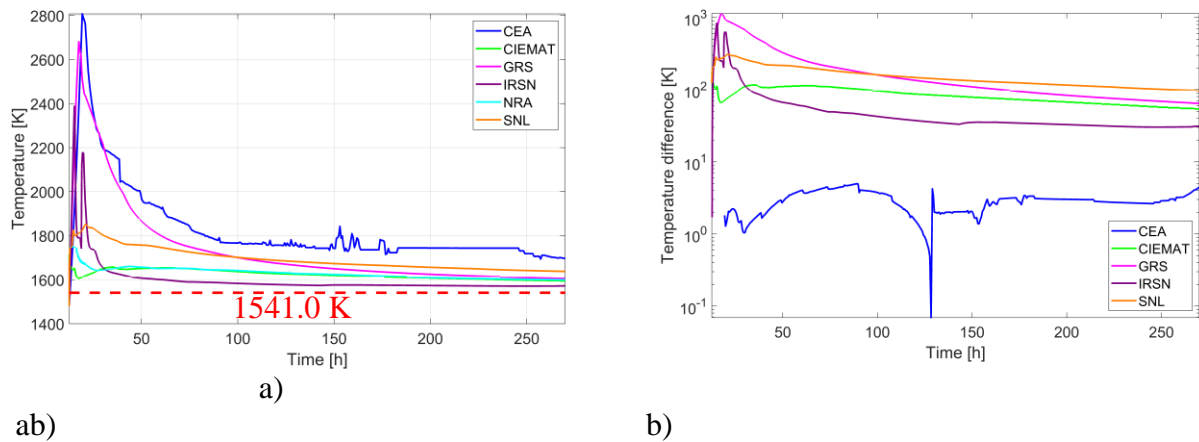
$\varphi_{towards\ concrete}$ gathers the heat flux released by the pool and the part released by the crust (owing to its decay power):

$$\varphi_{towards\ concrete} = h_{conv} (T_{pool} - T_{liquidus}) + \ddot{Q} e_{crust} \quad (4)$$

where h_{conv} is the convective HTC, $T_{liquidus}$ is the liquidus temperature at the pool composition e , $\rho_{l,conc}$ and $Cp_{l,conc}$ are the density and the specific heat of the liquid concrete respectively, \dot{Q} is the crust volumetric decay heat power (W/m^3) and e_{crust} its thickness (m). In equation (3), TOLBIAC-ICB considers also the sensible heat of the liquid concrete from the ablation to the pool temperature, which should be taken into account in other codes when doing the energy balance on the pool (initially at T_{pool}) with the incoming molten concrete at $T_{ablation}$.

5. RESULTS COMPARISON

Figure 7 a) presents the molten pool temperature evolution for all the codes. The molten pool temperature, whose initial value was 1481.346 K, has an initial spike increase up to over 2600 K due to chemical reactions of the metals contained in the initial debris. Once the chemical reactions of the initial metals in the corium ceases and the decay heat reduces, the temperature also reduces. However, it is noticeable that the temperature of the melt is always above the ablation temperature. Looking at equation (2) this implies that the erosion velocity is always greater than zero. Hence, the endless erosion experienced in BASF-2 and in this exercise as well. For the TOLBIAC-ICB code as well, the pool temperature is always larger than the liquidus temperature, which is used in the definition of the ablation velocity. The temperature difference in equation (2), that is to say $T_{pool} - T_{ablation}$ is plotted in Figure 7 b) for all codes, except for TOLBIAC-ICB where $T_{pool} - T_{liquidus}$ is plotted according to equation (4).



ab) **Figure 7 Corium temperature variation, a) whole temperature variation from 12.5 h to 270 h, b) temperature difference in equation (2) for all codes except equation (3) for TOLBIAC-ICB**

It is insightful from Figure 7 b) that the temperature difference in TOLBIAC-ICB, which drives the ablation velocity, is around two orders of magnitude lower than in the other codes. The temperature evolution is relatively similar in all calculations which asymptotically tend towards the ablation temperature, except for the CEA case which can be attributed to the different assumptions of the interface temperature as $T_{liquidus}$. The assumption that the interface temperature is equal to $T_{liquidus}$ indeed tends to generate a larger pool temperature. Figure 8 shows the normalized interface temperature, in equation (4) highlighting the different assumptions: The TOLBIAC-ICB code assumes that the interface temperature equals $T_{liquidus}$ while for the other codes is a function of the melt composition and temperature.

$$T_{interface}^* = \frac{T_{interface} - T_{solidus}}{T_{liquidus} - T_{solidus}} \quad (4)$$

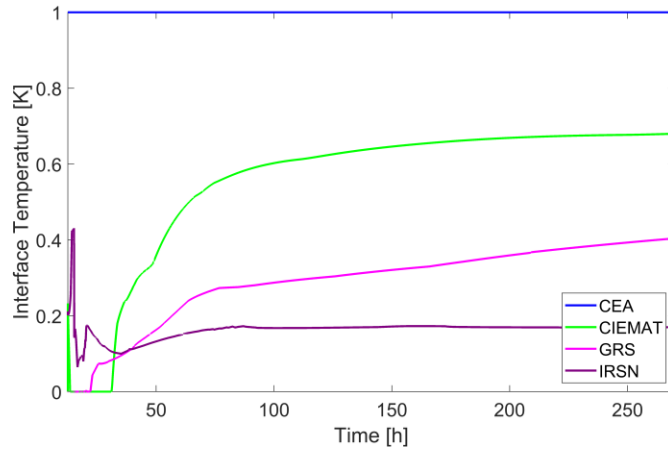


Figure 8 Normalized top interface temperature

Despite the molten pool temperature difference among some simulations, it is remarkable that the cavity erosion pattern is very similar among all the simulations. This result is reflected in the shape of concrete erosion presented in Figure 9 where the cavity size both vertically and radially grows continuously with a similar trend for all the calculations until 270 h. The same conclusion is supported by the ablation velocity evolution presented Figure 10 showing a very similar value for all calculations.

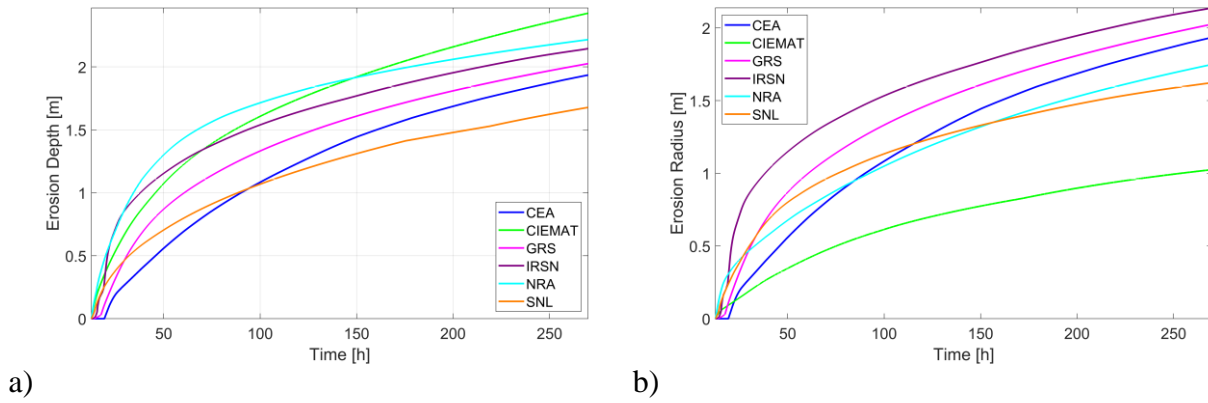


Figure 9 Maximum concrete erosion a) vertically and b) radially

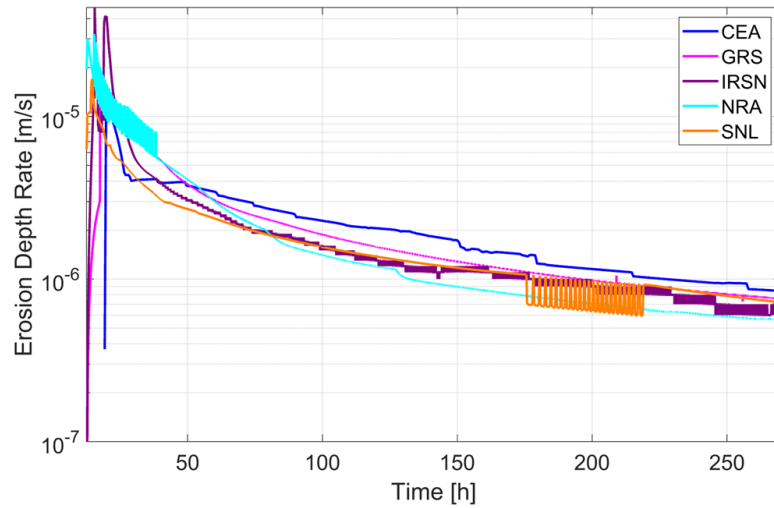


Figure 10 Vertical ablation velocity

This result appears clearer if we consider equations (2) and (3) heat transfer towards the concrete presented in Figure 11. In TOLBIAC-ICB, despite having the temperature difference always lower than other codes, the HTC is larger because it considers only the convective HTC which is proportional to the surface velocity of gases released due to the decomposition of concrete. In MEDICIS and the AC², the effective HTC is limited by the assumptions on the slag HTC which is the order of magnitude 10² [W/m²K]. However, something should be clarified as from 100 h the HTC in TOLBIAC-ICB reduces to a similar value as the other codes.

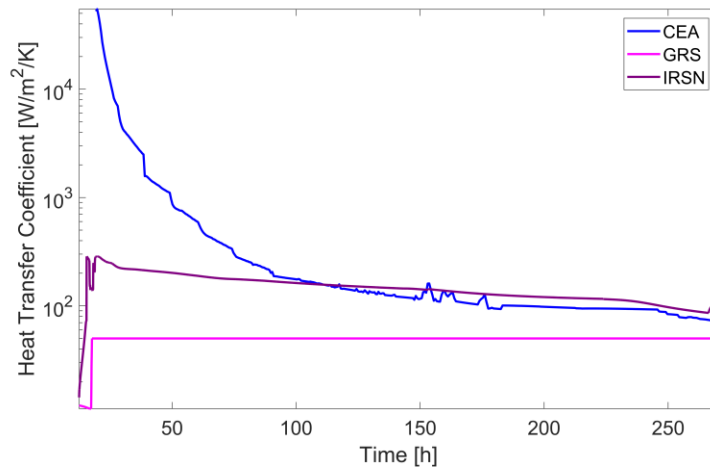


Figure 11 Effective heat transfer coefficient from the molten pool to the concrete

6. DISCUSSION

The results show that, as the definition of the heat removed from the top surface is lower than the decay heat the pool temperature will be always higher than the decomposition temperature, hence resulting always in a positive ablation velocity. This condition leads the predicted ablation at 270 h from the beginning of the accident to exceed the size of the pedestal walls as shown qualitatively in Figure 12.

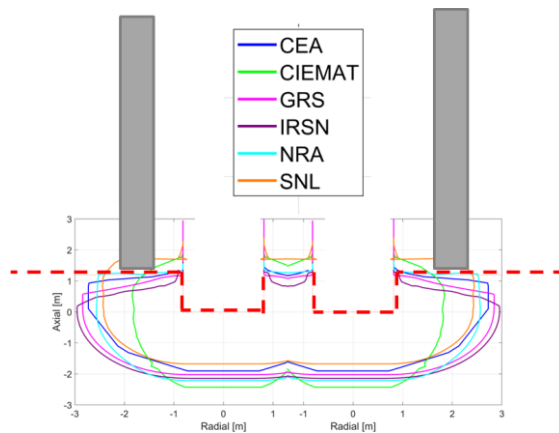


Figure 12 Predicted erosion end configuration in comparison with the pedestal walls

As the condition predicted in Figure 12 seems unrealistic the maybe three contributions that need to be taken into considerations for a more realistic simulation. First the decay heat employed in the simulation (presented in Figure 3) might be overpredicted as still debate exists on the amount of semi-volatile gases released from a hot corium. Second the heat losses on the surface might be larger than we compute, in particular in case the ablation temperature of the concrete were higher than what it is assumed, maintaining a larger debris temperature. Finally, the heat losses to the concrete, at the moment considered adiabatic, might not be negligible in such long transient and could represent a continuous heat sink to stop the erosion. Work is ongoing to estimate the heat flux introduced by the consideration of the heat conduction with moving boundary. Future work in the subsequent project of the OECD/NEA, the FACE project, will address these three main uncertainties, which is to say, the initial decay heat in the debris, the decomposition temperature and energy and the heat losses due to conduction in the concrete.

7. CONCLUSION

The analytical benchmark shows that even with controlling boundary and initial conditions, all the SA codes compute unlimited MCCI. The main results of erosion and ablation rate are very consistent with all the codes despite few differences among them, in particular in the modeling assumptions proposed by the TOLBIAC-ICB code. The fundamental modeling equations show clearly that the continuous erosion occurs because the overall heat losses and decay heat are not in balance, with the decay heat always above the losses to the surroundings. In the final discussion three main points to be considered for the future modeling in order to predict a condition in which MCCI might stop are: 1) the overall decay heat, 2) the concrete decomposition temperature and 3) the heat flux due to conduction through concrete.

8. REFERENCES

- [1] M. Pellegrini, L. Herranz, M. Sonnenkalb, T. Lind, Y. Maruyama, R. Gauntt, N. Bixler, A. Morreale, K. Dolganov, T. Sevón, D. Jacquemain, C. Journeau, J.H. Song, Y. Nishi, S. Mizokami, “Main Findings, Remaining Uncertainties and Lessons Learned from the OECD/NEA BSAF Project” *Nuclear Technology*, **206** (9), pp. 1449-1463 (2020)
- [2] L.E. Herranz, M. Pellegrini, T. Lind, M. Sonnenkalb, L. Godin-Jacqmin, C. López, K. Dolganov, F. Cousin, H. Tamaki, T.W. Kim, H. Hoshi, N. Andrews, T. Sevón, “Overview and outcomes of the OECD/NEA benchmark study of the accident at the Fukushima Daiichi NPS (BSAF) Phase 2 – Results of severe accident analyses for Unit 1” *Nuclear Engineering and Design*, **369**, (2020)
- [3] Sonnenkalb, M., Pellegrini, M., Herranz, L.E., Lind, T., Morreale, A.C., Kanda, K., Tamaki, H., Kim, S.I., Cousin, F., Fernandez Moguel, L., Andrews, N., Sevón, T. Overview and outcomes of the

- OECD/NEA benchmark study of the accident at the Fukushima Daiichi NPS (BSAF), phase 2 – Results of severe accident analyses for unit 2 (2020) Nuclear Engineering and Design, **369**, (2020)
- [4] Lind, T., Pellegrini, M., Herranz, L.E., Sonnenkalb, M., Nishi, Y., Tamaki, H., Cousin, F., Fernandez Moguel, L., Andrews, N., Sevon, T. Overview and outcomes of the OECD/NEA benchmark study of the accident at the Fukushima Daiichi NPS (BSAF), Phase 2 – Results of severe accident analyses for unit 3 Nuclear Engineering and Design, **376** (2021)
- [5] Luxat D.L., Kalinich D.A., Hanophy J.T., Gauntt R.O., Wachowiak, R.M, MAAP-MELCOR Crosswalk Phase 1 Study, Nuclear Technology, **196**:3, 684-697, (2016)
- [6] “OECD/NEA State of the Art Report on Molten Corium Concrete Interaction and Ex-Vessel Molten Core Coolability”, (2017)
- [7] Seiler N, Journeau C, Pellegrini M, Advanced analyses of Molten Core Corium Interaction with TOLBIAC-ICB at FUKUSHIMADAIICHI UNIT 1 in the framework of the ARC-F Project, FDR2022-1070, International Topical Workshop on Fukushima Decommissioning Research, Oct 14-16, 2022. J-Village, Naraha, Fukushima, Japan
- [8] Bonnet, J.-M. (1999), Thermal hydraulic phenomena in corium pools for ex-vessel situations: The BALI experiment. OECD workshop on ex-vessel coolability, FZKA 64753. Karlsruhe, Germany.
- [9] Bonnet, J.-M. (2000), Thermal hydraulic phenomena in corium pools for ex-vessel situations: the BALI experiment. ICONES. Baltimore, Maryland, USA.